Electronic Supplementary Material (ESI) for RSC Advances.

Enhanced active oxidative species generation over Fe-doping defective TiO_2 nanosheets for boosted photodegradation

Xintong Gao[a], Shuai Zhang[b], Jingchao Liu[c], Shiqi Xu[a] and Zenghe Li*[a]

Materials

Tetrabutyl titanate ($Ti(OBu)_4$), tetracycline hydrochloride (TC-HCl), ethylenediaminetetraacetic acid (EDTA) and bulk anatase TiO_2 were purchased from Aladdin Co., Ltd. Iron(III) nitrate nonahydrate ($Fe(NO_3)_3 \cdot 9H_2O$) and tertiary butyl alcohol (TBA) were obtained from Tianjin Fuchen Chemical Reaction Factory. The $Ti(OBu)_4$ and $Fe(NO_3)_3 \cdot 9H_2O$ were of analytical grade. Anhydrous ethanol, hydrofluoric acid (HF, 40 wt.%), and hydrogen peroxide (H_2O_2, 30wt.%) were purchased from Beijing Chemical Corporation. Rhodamine B (RhB) and p-benzoquinone (PBQ) were obtained from Sinopharm Chemical Reagent Co., Ltd. Ultra-pure water was used in all experiments.

Synthesis of X%-TiO_2 nanosheets *(where X% is the mole percent of Fe, expressed* as *100%× mol Fe / mol Ti)*

In a typical synthesis, 0.1685 g, 0.2808 g, 0.3931 g, 0.5054 g of $Fe(NO_3)_3 \cdot 9H_2O$ were added into anhydrous ethanol (40 mL) containing $Ti(OBu)_4$ (10 mL) and HF (1.2 mL), respectively. After stirring for 30 min, the solution was transferred into a stainless steel autoclave (100 mL) and then heated at 180 ^oC for 2 h. The products were collected by centrifugation and washed repeatedly with ultra-pure water. Finally, the products were dried at 60 ^oC under vacuum for 24 h.

Photocatalysts characterization

XRD patterns for photocatalysts were recorded by X-ray diffractometer (XRD, Bruker D8 Advance). The morphology of photocatalysts was characterized using a high-resolution transmission electron microscopy (HRTEM, JEOL-2100). Elemental analyses were obtained on inductively coupled plasma atomic emission spectroscopy (ICP-AES-7500, SHIMADZU). Chemical composition analyses were performed using a scanning transmission electron microscope (STEM, FEI Tecnai G2 F30) equipped with energy dispersive X-ray (EDX). Raman spectra were collected on Renishaw in Via spectrometer system. X-ray photoelectron spectroscopy (XPS) was performed on a KRATOS AXIS SUPRA system equipped with an Al Kα X-ray source. Brunauer-Emmett-Teller (BET) surface areas and N_2 physisorption isotherms were measured with a surface area and porosity analyzer (ASAP 2460t, Micromeritics), using liquid

nitrogen adsorbent at 77 K. Ultraviolet-Visible diffuse reflectance spectra (UV-DRS) were measured on a spectrophotometer (UV-3600, Shimadzu) using $BaSO_4$ as the reflectance standard. Photoluminescence spectra (PL) were obtained at room temperature using a fluorescence spectrophotometer (FLS700, Hitachi) (EM Start WL: 260.0 nm). Electron paramagnetic resonance (EPR) spectra were obtained on a Bruker EPR-E500 spectrometer. The thickness of the 3.5%-TiO_2 nanosheets was determined by atomic force microscopy (AFM) (Bruker FastScan).

Photocatalytic activity evaluation

The photocatalytic performance of all the as-prepared samples was investigated by measuring the degradation rate of RhB aqueous solution (10 mg L^{-1}) and TC-HCl aqueous solution (20 mg L^{-1}) under simulated sunlight irradiation (300 W xenon lamp, CEL-HXF300, Beijing Zhongjiao Jinyuan Technology Co., Ltd.). In each photocatalytic reaction, 80 mg photocatalysts and 1.5 mmol H_2O_2 were added into an aqueous RhB solution of 80 mL, and then the suspensions were stirred in the dark for 40 min to reach the adsorption-desorption equilibrium between photocatalysts and RhB solutions. Under light irradiation, 4 mL of RhB solution was sampled at 5 min interval and filtered to remove the photocatalysts for optical absorbance measurements. To analogous, 10 mg sample and 1.5 mmol H_2O_2 were added into an aqueous TC-HCl solution of 80 mL, and then the suspension was stirred in the dark for 40 min to reach the adsorption-desorption equilibrium between photocatalysts and TC-HCl solutions. During irradiation, 4 mL of TC-HCl solution was sampled at 10 min interval and filtered to remove the photocatalysts for optical absorbance measurements. The absorbance of reaction solution was measured with a UV-vis spectrophotometer (UVmini-1240, Shimadzu), and the concentration of pollutants was determined by the RhB and TC-HCl standard curve. According to Beer's law, the absorbance at 553 nm (the characteristic absorption wavelength of RhB) and 357 nm (the characteristic absorption wavelength of TC-HCl) were proportional to the concentration of RhB and TC-HCl in the reaction solution, respectively. Furthermore, the kinetic behaviors of photocatalysts were investigated through a pseudo-first-order model, $\ln[C/C_0] = -kt + \alpha$. Here, C_0 and C present the initial concentration before irradiation and the residual

concentration of RhB and TC-HCl solution after irradiation for *t* min, respectively, and *k* is the apparent rate constant.

In the cycle test experiments, photocatalytic performance of 3.5%-TiO_2 was evaluated by performing 20 min of RhB photodegradation and 60 min of TC-HCl photodegradation experiments. Then the photocatalysts were recovered from the reaction solution, repeatedly washed with ethanol/ultrapure water and dried, and reused in photodegradation tests (ethanol was completely removed from the photocatalysts before the photocatalytic testing). A total of 4 such reaction cycles were performed (with approximately the same amount of photocatalyst used in each reaction cycle).

Active oxidative species (AOS) trapping

Generally, holes (h^+), superoxide radical ($\bullet O_2^-$), and hydroxyl radicals (•OH) are considered as predominant AOS for dyes and antibiotics photodegradation.[1-2] To investigate the predominant AOS involved, radicals trapping experiments were performed, which is similar to former photocatalytic activity measurement. In this process, TBA (10 mmol L^{-1}), PBQ (10 mmol L^{-1}), and EDTA (10 mmol L^{-1}) were used as the scavengers for •OH, $\bullet O_2^-$, and h^+, respectively.

EPR tests

EPR tests were performed by using a Bruker EPR-E500 spectrometer operating at room temperature. The $\bullet O_2^-$ radicals can be captured by 5,5-dimethyl-l-pyrroline N-oxide (DMPO). For the detection of DMPO-$\bullet O_2^-$ adducts, 20 mg of 3.5%-TiO_2 photocatalyst and a small amount of H_2O_2 were added into 50 μL of 5 wt.% DMPO/DMSO solution.

Electrochemical measurements

The electrochemical measurements were performed on a CHI 660E electrochemical workstation equipped with a three-electrode cell. The working electrode was a glassy carbon electrode coated with catalysts, the counter electrode was a platinum foil, and the reference electrode was a saturated Ag/AgCl electrode with saturated K_2SO_4 (1 mol L^{-1}) as the electrolyte. The electrochemical impedance spectroscopy (EIS) measurements were conducted over a frequency range 0.01-10^5 Hz without light. Photocurrent measurements and Mott-Schottky experiments were conducted with voltage range from -1.5 V-0 V, in accordance with procedures previous work.[3]

Poisson's equation can be solved to give the Mott–Schottky equation:[4]

$$\frac{1}{C^2} = \frac{2}{\varepsilon\varepsilon_0 e A^2 \mathrm{N_D}}\left(V - V_{\mathrm{fb}} - \frac{k_B T}{e}\right)$$

Where C and A are the interfacial capacitance and area, respectively, N_D the number of donors, V the applied voltage, k_B is Boltzmann's constant, T is the temperature, and e is the electronic charge. Therefore, a plot of C^{-2} against voltage should yield a straight line from which V_{fb} can be determined from the intercept on the voltage axis.

The value of N_D is determined from the slope with knowledge of ε and A.[5-6]

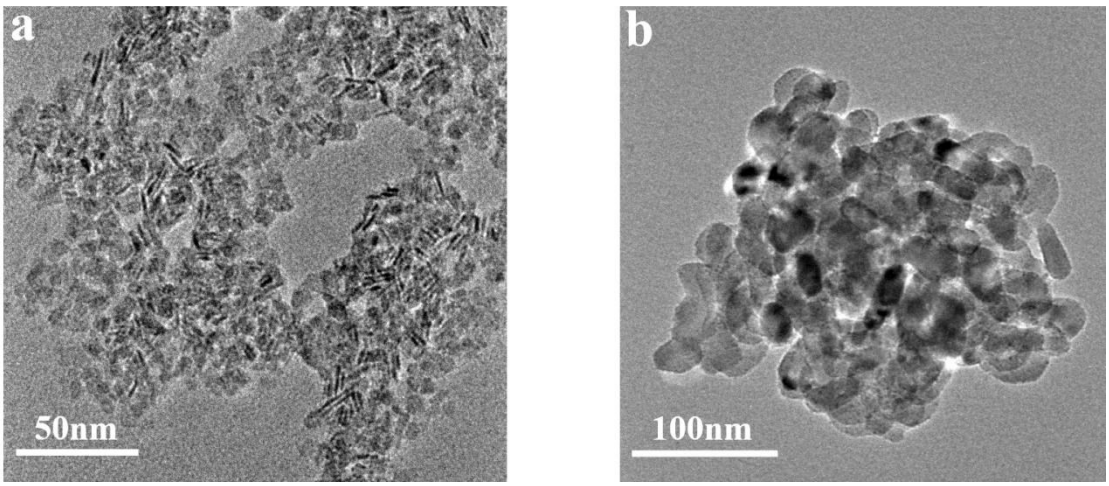

Fig. S1 TEM images of (a) 0%-TiO_2 nanosheets and (b) Bulk-TiO_2.

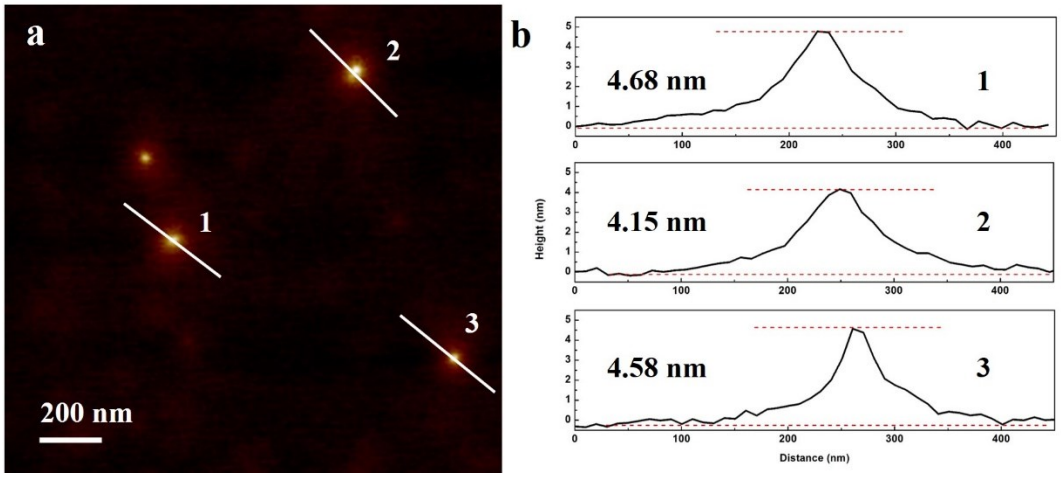

Fig. S2 (a) AFM image and (b) corresponding height profiles of 3.5%-TiO_2 nanosheets (the numbers 1, 2 and 3 correspond to the line scan number in (a).

Table S1 ICP-AES data for the actual contents of Fe doping in X%-TiO_2 nanosheets (X = 1.5, 2.5, 3.5, 4.5).

sample	cFe (ppm)	cTi (ppm)	X (%) (X = Fe/Ti molar ratio)
1.5%-TiO_2	4.716	233.2	1.70%
2.5%-TiO_2	7.833	239.1	2.75%
3.5%-TiO_2	10.93	236.4	3.89%
4.5%-TiO_2	12.37	216.3	4.80%

cFe and cTi represent the concentration of metal ions in the catalysts solution.

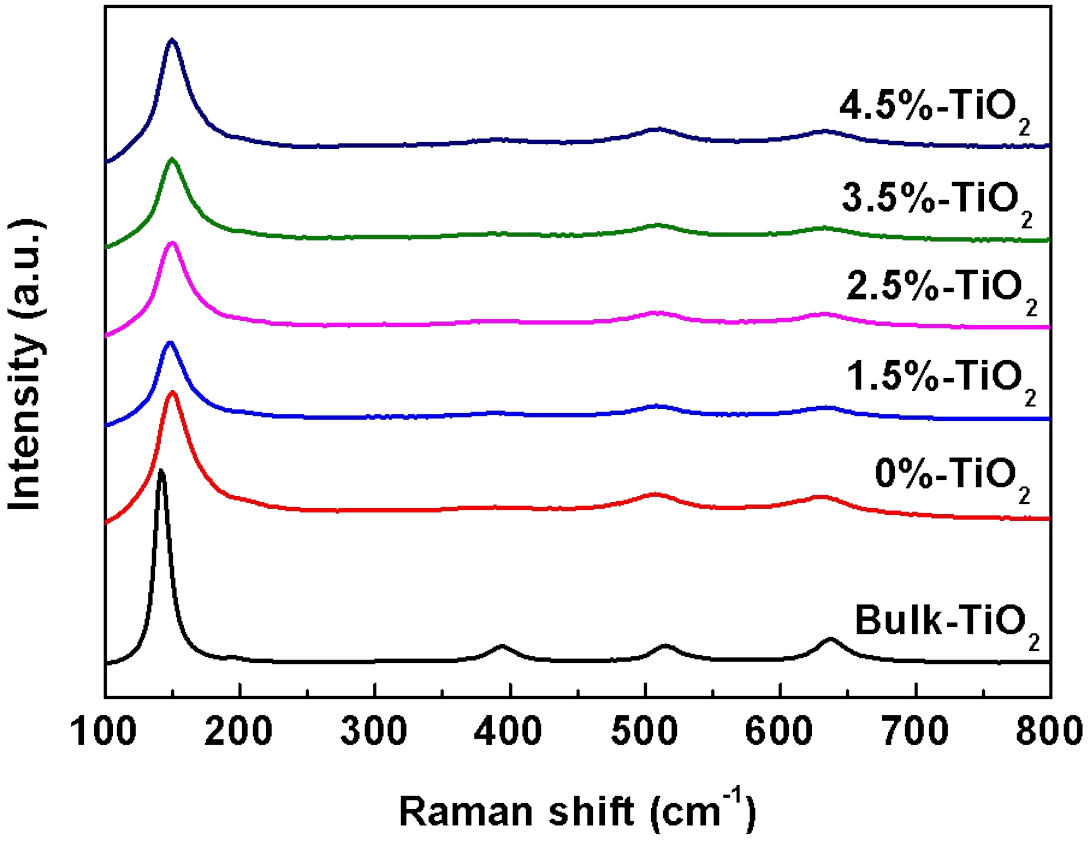

Fig. S3 (a) Raman spectra for X%-TiO_2 nanosheets (X=0, 1.5, 2.5, 3.5, 4.5) and Bulk-TiO_2.

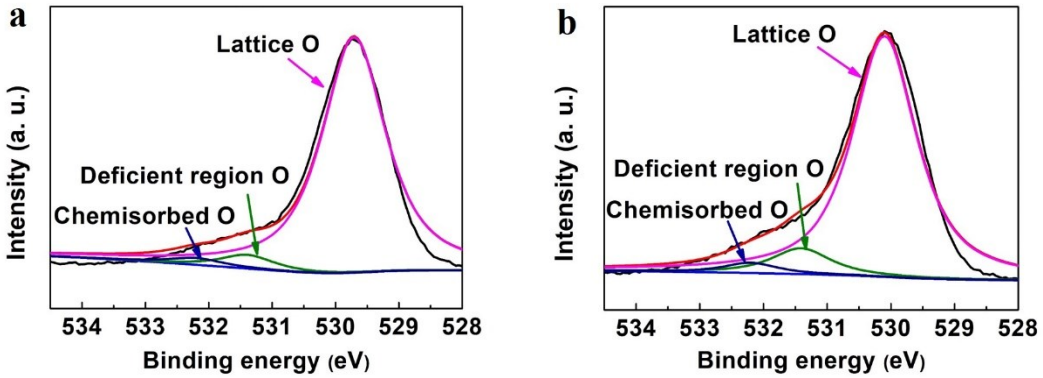

Fig. S4 XPS spectra of O 1s in the (a) Bulk-TiO_2 and (b) 0%-TiO_2 nanosheets.

Table S2 Comparison of RhB photodegradation of various photocatalysts reported.

Catalyst	Light source	The amount of catalyst (mg)	RhB concentration (ppm)	Photocatalytic degradation rate (min^{-1})	Reference
3.5%-TiO_2	300 W xenon lamp	80	10	0.3073	This work
Ce-doped TiO_2	300 W xenon lamp	400	10	0.00348	[7]
B-doped BiOCl	350W xenon lamp	10	10	0.01704	[8]
N-doped $ZnWO_4$	sunlight	10	10	0.1708	[9]
B-doped Bi_2MoO_6	250 W halogen Lamp	20	5	0.016	[10]
Pt-doped TiO_2	220W mercury lamp	3	10	0.0053	[11]
I/C-doped TiO_2	300 W Xe arc lamp	50	20	0.1600	[12]
C-N-S-doped TiO_2	8 W UV lamp	20	10	0.01234	[13]
Fe–N–S-tri-doped TiO_2	500 W Xenon lamp	200	20	0.0291	[14]
C/N-doped Au/TiO_2	500 W xenon lamp	5	4.79	0.0071	[15]

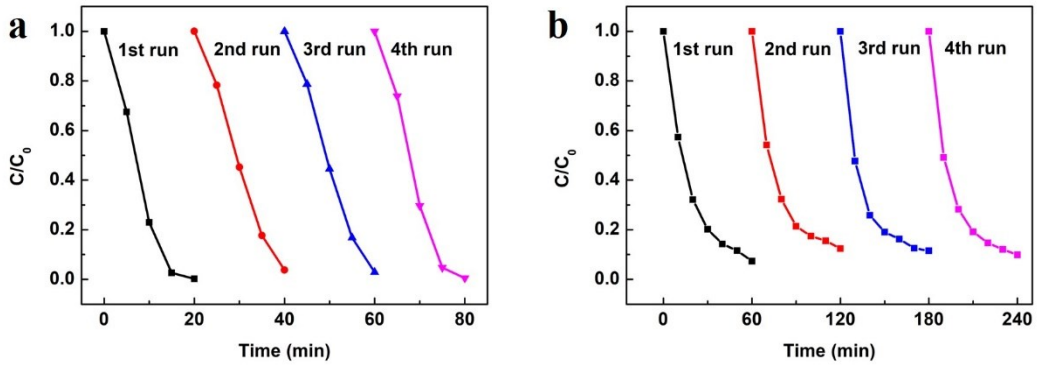

Fig. S5 Cycling runs of 3.5%-TiO_2 nanosheets for photocatalytic degradation of (a) RhB and (b) TC-HCl solution.

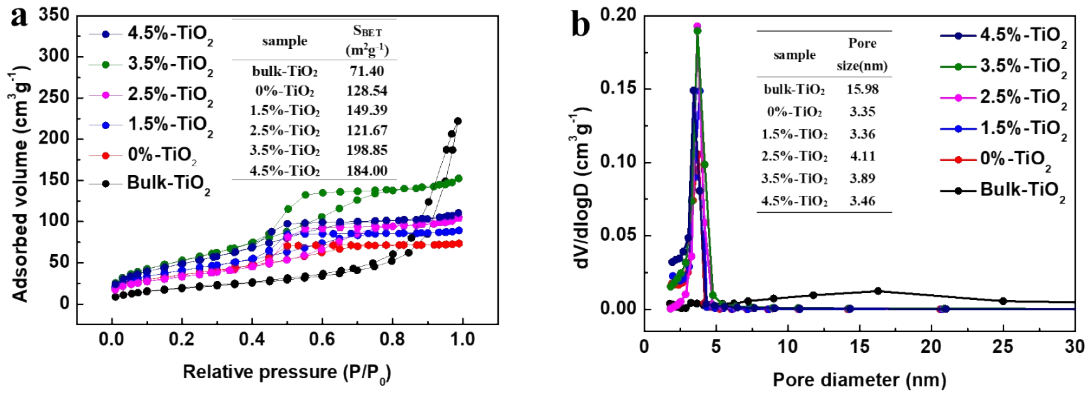

Fig. S6 (a) N_2 adsorption-desorption isotherms of X%-TiO_2 nanosheets and Bulk-TiO_2. (b) Pore size distribution of X%-TiO_2 nanosheets and Bulk-TiO_2.

According to the International Union of Pure and Applied Chemistry (IUPAC) classification,[16] the isotherm curves of Bulk-TiO_2 can be classified as Type-II isotherms, which manifested the nature of micropores.[17] The X%-TiO_2 nanosheets showed Type-IV isotherms with H2-type hysteresis in the relative pressure of 0.4-0.8, which confirmed the presence of mesopores in the ultrathin X%-TiO_2 nanosheets.

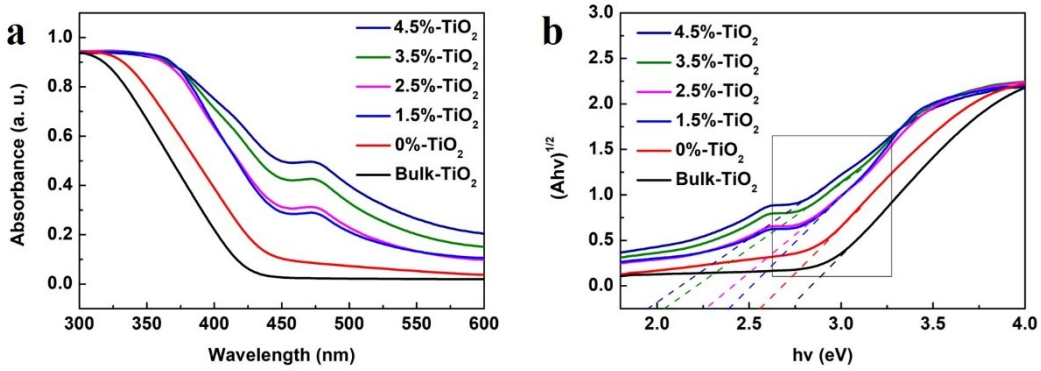

Fig. S7 (a) UV-DRS data and (b) Tauc plots for X%-TiO_2 nanosheets and Bulk-TiO_2.

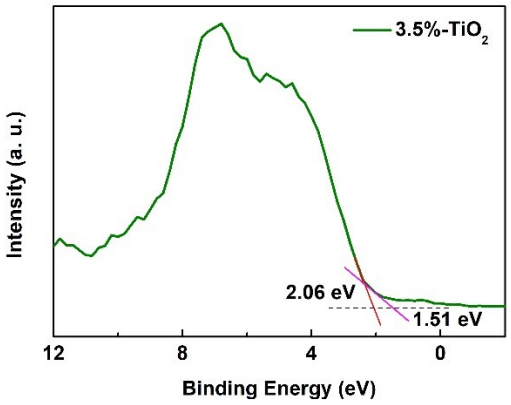

Fig. S8 XPS valence band spectra of 3.5%-TiO_2.

According to the UV-DRS (Fig. S7a-b) and Mott-Schottky diagram (Fig. 5d), the band gap and conduction band (CB) position of 3.5%-TiO_2 nanosheets were estimated to be 2.04 eV and -0.54 eV, respectively. The valence band (VB) position of 3.5%-TiO_2 nanosheets was thus calculated to be about 1.50 eV. The VB maximum of 3.5%-TiO_2 was also measured by XPS valance spectra, a VB edge was 2.06 eV and a band tailing was 1.51 eV (Fig. S8).[18-20] In addition, the band edge energy (E_{CB}, E_{VB}) of 3.5%-TiO_2 nanosheets was further calculated according to the empirical equation as follow:[21]

$$E_{VB} = \chi - E^C + \frac{1}{2}Eg$$

where χ represents the electronegativity of the semiconductors (here, the value of χ is 5.18 eV for 3.5%-TiO_2),[22] E^C is the standard hydrogen electrode scale (NHE) (E^C = 4.5 eV)[21] and Eg is the bandgap for 3.5%-TiO_2 (Eg = 2.04 eV). The calculated E_{VB} for 3.5%-TiO_2 is found to be about 1.70 eV. Considering the above calculation results, experimental data and inevitable experimental errors, the VB position of 3.5%-TiO_2 is inferred between 1.50-2.06 eV. According to the previous reports, some typical semiconductor photocatalysts with VB position between 1.50-2.06 eV can also generate holes with sufficient oxidation potential for the photodegradation of RhB and TC-HCl in water,[23-24] Moreover, both superoxide radical ($\bullet O_2^-$) and photo-generated holes contributed to the photodegradation of RhB and TC-HCl, as proved by radicals trapping experiments and EPR tests (Fig. 6a-c). Considering that both $\bullet O_2^-$ and the photo-

generated holes of 3.5%-TiO_2 possess sufficient oxidation ability to oxidize RhB and TC-HCl, so it would be safe to deduce that the 3.5%-TiO_2 nanosheets has sufficient oxidation for oxidizing the pollutants.

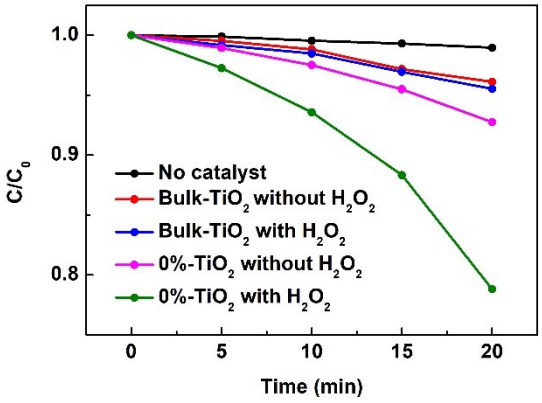

Fig. S9 Time profiles of RhB degradation for 0%-TiO_2 nanosheets and Bulk-TiO_2 with or without H_2O_2.

To explore the role of H_2O_2 in the photocatalytic reaction, we carried out a series of control experiments. As shown in Fig. S9, when there is no catalyst and only H_2O_2 in the reaction system, the concentration of RhB remained basically unchanged after 20 min light irradiation, which means that H_2O_2 itself cannot achieve the RhB photodegradation without the aid of photocatalysts. For Bulk-TiO_2, regardless of whether H_2O_2 is added to the reaction solution, the removal efficiency of RhB was almost unchanged after 20 min light irradiation, while the 0%-TiO_2 nanosheets displayed improved degradation performance in the presence of H_2O_2, with the RhB removal efficiency of 19.2%, which is higher than that for 0%-TiO_2 in the absence of H_2O_2. Since ultrathin 0%-TiO_2 nanosheets possessed higher concentration of Vo than Bulk-TiO_2, it is assumed that H_2O_2 can play a role in boosting the photocatalytic degradation only in the presence of photocatalysts rich in Vo. This inference may also be valid for 3.5%-TiO_2 nanosheets.

In the photocatalysis process, H_2O_2 can be reduced to •OH by photo-generated electrons,[25-26] while it can also be oxidized to $\bullet O_2^-$ by photo-generated holes.[25, 27-28] Through radical capture experiments, the main oxidative species for RhB/TC-HCl degradation by 3.5%-TiO_2 were identified to be holes and $\bullet O_2^-$, rather than •OH (Fig. 6a-b). Thence, it is possible that Vo-rich TiO_2 nanosheets converted H_2O_2 into more $\bullet O_2^-$ which contribute to the pollutants degradation. The above experimental results

manifested that H_2O_2 could not only participate in the Fenton reaction, but also be oxidized to $\bullet O_2^-$ by photo-generated holes in the assistance of Vo-rich TiO_2 photocatalysts, thereby further promoting the degradation of RhB or TC-HCl.

References

1 X. Zhang, L. Li, Y. Zeng, F. Liu, J. Yuan, X. Li, Y. Yu, X. Zhu, Z. Xiong, H. Yu and Y. Xie, *ACS Appl. Nano Mater.*, 2019, **2**, 7255-7265.

2 Y. Wang, L. Rao, P. Wang, Z. Shi and L. Zhang, *Appl. Catal. B: Environ.*, 2020, **262**, 118308.

3 Y. Zhao, Y. Zhao, G. I. N. Waterhouse, L. Zheng, X. Cao, F. Teng, L.-Z. Wu, C.-H. Tung, D. O'Hare and T. Zhang, *Adv. Mater.*, 2017, **29**, 1703828.

4 Y. Zhao, Y. Zhao, R. Shi, B. Wang, G. I. N. Waterhouse, L.-Z. Wu, C.-H. Tung and T. Zhang, *Adv. Mater.*, 2019, **31**, 1806482.

5 K. Gelderman, L. Lee and S. W. Donne, *J. Chem. Educ.*, 2007, **84**, 685.

6 J. Chen, B. Li, J. Zheng, S. Jia, J. Zhao, H. Jing and Z. Zhu, *J. Phys. Chem. C.*, 2011, **115**, 7104-7113.

7 Z. Liu, L. Xing, H. Ma, L. Cheng, J. Liu, J. Yang and Q. Zhang, *Environ. Prog. Sustain. Energy.*, 2017, **36**, 494-504.

8 C. Yu, H. He, Q. Fan, W. Xie, Z. Liu and H. Ji, *Sci. Total Environ.*, 2019, **694**, 133727.

9 Y. A. Sethi, C. S. Praveen, R. P. Panmand, A. Ambalkar, A. K. Kulkarni, S. W. Gosavi, M. V. Kulkarni and B. B. Kale, *Catal. Sci. Technol.*, 2018, **8**, 2909-2919.

10 M. Wang, J. Han, P. Guo, M. Sun, Y. Zhang, Z. Tong, M. You and C. Lv, *J. Phys. Chem. Solids.*, 2018, **113**, 86-93.

11 R. Pol, M. Guerrero, E. García-Lecina, A. Altube, E. Rossinyol, S. Garroni, M. D. Baró, J. Pons, J. Sort and E. Pellicer, *Appl. Catal. B-Environ.*, 2016, **181**, 270-278.

12 J.-C. Wang, H.-H. Lou, Z.-H. Xu, C.-X. Cui, Z.-J. Li, K. Jiang, Y.-P. Zhang, L.-B. Qu and W. Shi, *J. Hazard. Mater.*, 2018, **360**, 356-363.

13 X. Cheng, X. Yu and Z. Xing, *J. Phys. Chem. Solids*, 2013, **74**, 684-690.

14 X. Xu, X. Zhou, L. Zhang, L. Xu, L. Ma, J. Luo, M. Li and L. Zeng, *Mater. Res. Bull.*, 2015, **70**, 106-113.

15 Y. Li, S. Cao, A. Zhang, C. Zhang, T. Qu, Y. Zhao and A. Chen, *Appl. Surf. Sci.*, 2018, **445**, 350-358.

16 D. X. Martínez Vargas, J. Rivera De la Rosa, C. J. Lucio-Ortiz, A. Hernández-Ramirez, G. A. Flores-Escamilla and C. D. Garcia, *Appl. Catal. B-Environ.*, 2015, **179**, 249-261.

17 T. Wang, W. Li, D. Xu, X. Wu, L. Cao and J. Meng, *Appl. Surf. Sci.*, 2017, **426**, 325-332.

18 X. Chen, L. Liu, P. Y. Yu and S. S. Mao, *Science*, 2011, **331**, 746.

19 A. Naldoni, M. Allieta, S. Santangelo, M. Marelli, F. Fabbri, S. Cappelli, C. L. Bianchi, R. Psaro and V. Dal Santo, *J. Am. Chem. Soc.*, 2012, **134**, 7600-7603.

20 S. G. Ullattil and R. M. Ramakrishnan, *ACS Appl. Mater. Interfaces*, 2018, **1**, 4045-4052.

21 Zhang, L. Li, Y. Zeng, F. Liu, J. Yuan, X. Li, Y. Yu, X. Zhu, Z. Xiong, H. Yu and Y. Xie, *ACS Appl. Nano Mater.*, 2019, **2**, 7255-7265.

22 M. A. Majeed Khan, R. Siwach, S. Kumar and A. N. Alhazaa, *Opt. Laser Technol.*, 2019, **118**, 170-178.

23 R. Zhao, X. Sun, Y. Jin, J. Han, L. Wang and F. Liu, *J. Mater. Sci.*, 2019, **54**, 5445-

5456.
24 Y. Wang, X. Yang, T. Ye, C. Xu, F. Xia and D. Meng, *J. Electron. Mater.*, 2017, **46**, 1598-1606.
25 T. Hirakawa and Y. Nosaka, *Langmuir*, 2002, **18**, 3247-3254.
26 J. Rabani, K. Yamashita, K. Ushida, J. Stark and A. Kira, *J. Phys. Chem. B*, 1998, **102**, 1689-1695.
27 L. Sun and J. R. Bolton, *J. Phys. Chem.*, 1996, **100**, 4127-4134.
28 Y. Nosaka and A. Nosaka, *Chem. Rev.*, 2017, **117**, 11302−11336.